

## **OPEN ACCESS**

# Suppression of Impedimetric Baseline Drift for Stable Biosensing

To cite this article: Hilena F. Gezahagne et al 2022 ECS Sens. Plus 1 031605

View the article online for updates and enhancements.

## You may also like

- Contact between Garnet-Type Solid Electrolyte and Lithium Metal Anode: Influence on Charge Transfer Resistance and Short Circuit Prevention Rajendra Hongahally Basappa, Tomoko Ito and Hirotoshi Yamada
- Fully printed and flexible multi-material electrochemical aptasensor platform enabled by selective graphene biofunctionalization Shay Goff Wallace, Michael C Brothers, Zachary E Brooks et al.
- Degradation Mechanisms and Electron Kinetics Analysis in Aging Dye Sensitized Solar Cell Using Electrochemical Impedance Spectroscopy
  Szu Cheng Lai, Kang Nuo Peh Connor and Lin Ke





# Suppression of Impedimetric Baseline Drift for Stable Biosensing

Hilena F. Gezahagne, <sup>1,2</sup> Eleanor L. Brightbill, <sup>2</sup> Decarle S. Jin, <sup>2</sup> Siamalan Krishnathas, <sup>2</sup> Billyde Brown, <sup>3</sup> Mark H. Mooney, <sup>4</sup> Alan O'Riordan, <sup>5</sup> Niamh Creedon, <sup>5</sup> Caoimhe Robinson, <sup>5</sup> and Eric M. Vogel <sup>2</sup>

Biosensors based on Electrochemical Impedance Spectroscopy (EIS) detect the binding of an analyte to a receptor functionalized electrode by measuring the subsequent change in the extracted charge-transfer resistance ( $R_{CT}$ ). In this work, the stability of a long chain alkanethiol, 16-mercaptohexadecanoic acid was compared to that of a polymer-based surface linker, ortho-aminobenzoic acid (o-ABA). These two classes of surface linkers were selected due to the marked differences in their structural properties. The drift in  $R_{CT}$  observed for the native SAM functionalized gold electrodes was observed to correlate to the drift in the subsequent receptor functionalized SAM. This indicates the importance of the gold-molecule interface for reliable biosensing. Additionally, the magnitude of the baseline drift correlated to the percentage of thiol molecules improperly bound to the gold electrode as evaluated using X-ray Photoelectron Spectroscopy (XPS). Alternatively, the o-ABA functionalized gold electrodes demonstrated negligible drift in the  $R_{CT}$ . Furthermore, these polymer functionalized gold electrodes do not require a stabilization period in the buffer solution prior to receptor functionalization. This work emphasizes the importance of understanding and leveraging the structural properties of various classes of surface linkers to ensure the stability of impedimetric measurements.

© 2022 The Author(s). Published on behalf of The Electrochemical Society by IOP Publishing Limited. This is an open access article distributed under the terms of the Creative Commons Attribution 4.0 License (CC BY, http://creativecommons.org/licenses/by/4.0/), which permits unrestricted reuse of the work in any medium, provided the original work is properly cited. [DOI: 10.1149/2754-2726/ac8fa1]

Manuscript submitted July 13, 2022; revised manuscript received August 26, 2022. Published October 17, 2022.

Supplementary material for this article is available online

Enzyme-linked immunosorbent assays (ELISAs) have been one of the most dominant and widely utilized platforms for the detection of serological diseases. Extensive efforts have been made to optimize the performance and efficiency of ELISAs; however, several practical limitations remain.<sup>1,2</sup> ELISAs rely on trained laboratory personnel to perform the assay, often in a centralized laboratory which increases both the cost and time to actionable treatment. Additionally, ELISAs require the use of labeled reporter molecules such as florescent labels, which increases the operational complexity of the assay. 3-7 Today, commercially available label-free biosensing platforms such as surface plasmon resonance (SPR) and quartz crystal microbalance (QCM) are prevalent in many research laboratories, offering an alternative to ELISA-based screening approaches. 8–9,10 However, these techniques require expensive instrumentation and currently are not sufficiently high throughput to be amenable for many routine applications.

Alternatively, an electrochemical impedance spectroscopy (EIS) biosensor is a label-free platform that not only reduces operational complexity but has shown high sensitivity and can be mass produced at low cost. <sup>11–24</sup> EIS-based biosensors have a wide variety of potential applications ranging from medical care to food safety, where there is a heavy reliance on the rapid and accurate detection of biological and chemical species. Additionally, surface regeneration techniques can be optimized to ensure the reusability of these sensors. <sup>23</sup> This allows for the repeated detection of key biomarkers on one device. <sup>23</sup>

In EIS, the electrical impedance of a biological interface is measured under DC bias and AC oscillation.  $^{24}$  The charge transfer resistance ( $R_{CT}$ ) is extracted by fitting the Nyquist plot with an equivalent circuit model, such as the Randle circuit.  $^{24}$ 

One of the challenges associated with commercializing EIS based biosensors is the lack of stability and reproducibility associated with this technique.<sup>27</sup> EIS based biosensors detect the binding of an

analyte to a receptor functionalized Au electrode by measuring the subsequent change in  $R_{\rm CT}^{-25,27}$  Typically, electrochemical based biosensors consist of thiol functionalized gold electrodes. <sup>26,27</sup>

Recent publications have shown that a change in the measured R<sub>CT</sub> can be observed during continuous EIS measurements on a SAM functionalized gold electrode.<sup>27</sup> These thiol molecules are not stationary once adsorbed onto the gold electrode and may reorganize once placed in the measurement solution.<sup>27</sup> It is hypothesized that this SAM reorganization process is the cause of drift in the measured R<sub>CT</sub>. <sup>27</sup> Consequently, this baseline drift can be incorrectly attributed to a binding event.<sup>27</sup> Therefore, to accurately correlate an increase in the measured R<sub>CT</sub> to the attachment of the target analyte, it is essential that the baseline drift is suppressed prior to functionalization. Previous publications incorporated a conditioning step to ensure a stable R<sub>CT</sub> baseline prior to receptor functionalization and analyte attachment.<sup>27</sup> However, the primary challenge with this approach is the length of this conditioning step is dependent on the magnitude of the baseline drift. The magnitude of the baseline drift was found to vary from one electrode to the next. As a result, the length of the conditioning step required to reach a stable R<sub>CT</sub> baseline varied between electrodes. Therefore, this protocol cannot be easily translated for use in PoCTs. To effectively suppress the baseline drift in the measured R<sub>CT</sub>, it is important to understand what properties of these thiol-based SAMs contribute to their mobility.

The uniformity of SAMs has been shown to be dependent on three primary factors: the solution pH, the structural properties of the thiol molecules, and the impurities and intrinsic defects present in the underlying polycrystalline gold electrode. <sup>26,28–31</sup> The thiol molecules consist of three distinct components: the sulfur head group that forms a covalent S to Au bond (~50kcal/mol), the alkyl chain length which influences the SAM packing density, and the terminal functional group which is necessary for protein immobilization. <sup>26,28,31</sup>

An increase in the alkyl chain length increases the chain-to-chain Van der Waals interactions, which improves the packing density and subsequent uniformity of the SAM.<sup>26,30,31</sup> Molecular dynamic studies have shown that an increase in the alkyl chain length

<sup>&</sup>lt;sup>1</sup>School of Chemistry, Georgia Institute of Technology, Atlanta, Georgia 30332, United States of America

<sup>&</sup>lt;sup>2</sup>School of Materials Science and Engineering, Georgia Institute of Technology, Atlanta, Georgia 30332, United States of America

<sup>&</sup>lt;sup>3</sup>Georgia Tech Manufacturing Institute, Atlanta, Georgia 30332, United States of America

<sup>&</sup>lt;sup>4</sup>Institute for Global Food Security, School of Biological Sciences, Queen's University Belfast, Belfast, Northern Ireland BT9 5AG, United Kingdom

<sup>&</sup>lt;sup>5</sup>Nanotechnology Group, Tyndall National Institute, University College Cork, Cork T12 R5CP, Ireland

decreases the mobility of the thiol molecules in solution.<sup>32</sup> This is assumed to be due to the increased uniformity and crystallinity associated with long chain alkanethiol based SAMs.<sup>32</sup> Carboxylic acid terminal functional groups are typically used for biosensing applications due to the ease with which receptor proteins through amine reactive chemistry. 25,26,33,34 Despite their common use, carboxylic acid terminal functional groups are bulky and can interrupt the Van der Waals interactions between neighboring alkyl chains. Additionally, hydrogen bonding between neighboring carboxylic acid groups disrupts the uniformity of these SAMs. 26,33,35,36 The uniformity of these carboxylic acid terminated thiol based monolayers can be optimized by decreasing the concentration of the ethanolic thiol solution used to form the SAM. Decreasing the concentration of the ethanolic thiol solution decreases the propensity for hydrogen bonding between neighboring carboxylic acid terminal functional groups, thereby improving the uniformity of the SAM.

Additionally, intrinsic defects such as step edges and grain boundaries present in the underlying polycrystalline gold electrode induce subsequent defects in the SAM. <sup>26,29</sup> Although methods like annealing improve the crystallinity of the gold electrode, the defect density may be inconsistent across the surface of the electrode. The stability and reliability of a biosensor is dependent on the surface properties of the electrode and the structural properties of the adsorbed surface linker. Screen printed electrodes (SPEs) are small, disposable devices that have been successfully used to detect a wide variety of biomarkers. <sup>29,38–40</sup> Prior work by Butterworth et al. compared the sensitivity and reproducibility of commercially available SPEs to polycrystalline gold electrodes and thin-film gold electrodes. <sup>29</sup> The overall biosensor performance was found to be reliant on both the surface roughness and the subsequent SAM composition. <sup>29</sup> The overall performance of a biosensing platform has been shown to be heavily reliant on both the surface properties of the electrode and the structural properties of the surface linker. <sup>29</sup>

Previous work has shown that the use of short chain alkanethiols (mercaptohexanol) result in significant drift in the measured  $R_{\rm CT}$ . In this work, a long chain, alkanethiol (16-mercaptohexadecanoic acid) was used to form the SAM functionalized gold electrode. The long chain alkanethiol should form a more uniform SAM, as the long alkyl chains increase the chain-to-chain Van der Waals interactions which increases the packing density of the SAM. A range of experimental conditions for SAM formation including incubation times and concentration of the ethanolic thiol solution were investigated.

The stability of these surface linkers were studied under ambient conditions as it has been shown that thiol based SAMs decompose at elevated temperatures.<sup>51</sup> The elemental composition of the SAM functionalized gold electrodes were characterized via XPS. The magnitude of the baseline drift in the measured R<sub>CT</sub> was found to be inversely related to the percentage of properly bound S to Au. Similar to previously published work, the drift in the SAM functionalized electrode was suppressed through conditioning of the electrode via several hours of repeated EIS measurements. The length of the conditioning step was found to be dependent on the percentage of S bound to Au. A challenge associated with using these thiol-based SAMs is the magnitude of the measured drift varied from one electrode to the next, despite identical experiment protocols being used. Consequently, the required conditioning time needed to reach a stable R<sub>CT</sub> baseline varied from one electrode to the next. Additionally, the measured baseline drift associated with the SAM functionalized gold electrode was found to correlate to the drift in the subsequent receptor functionalized SAM. Thus, emphasizing the importance of reaching a stable R<sub>CT</sub> baseline prior to the attachment of the target analyte. Although the conditioning of the SAM functionalized electrode is necessary for reliable biosensing, it is not a practical solution that can be applied for use in electronic based point of care technologies (PoCTs).

To address the issues associated with thiol functionalized gold electrodes, a class of polymer-based surface linkers was

investigated. O-ABA, an organic conducting polymer, was deposited onto the gold electrodes via electrodeposition and the associated stability of EIS measurements was studied. O-ABA is a linear polymer chain, which has covalent bonds between neighboring aromatic groups. It is hypothesized that these covalent bonds, in addition to  $\pi$  to  $\pi$  stacking of the aromatic rings, will not allow for the deposited polymer to easily reorganize. Additionally, o-ABA does not depend on the S-Au bond to adsorb onto the sensor surface. Thus, by selecting a surface linker that is not dependent on the percentage of properly bound S-Au and the subsequent electrostatic repulsions between neighboring alkyl chains, the baseline drift should be effectively suppressed.

This class of organic, conducting polymers can have a variety of terminal functional groups (e.g., carboxyl, hydroxyl, amine)<sup>41</sup> that permits the attachment of a receptor protein through amine reactive cross-linker chemistry.<sup>25,33,34,42</sup>

The o-ABA functionalized gold electrodes show stability and reproducibility without the incorporation of a conditioning step prior to receptor functionalization. The receptor activity of this polymer functionalized electrode was confirmed via surface plasmon resonance measurements demonstrating their applicability for EIS-based PoCTs. <sup>25,42</sup>

### **Materials and Methods**

16-mercaptohexadecanoic acid [HS-(CH<sub>2</sub>)<sub>15</sub>COOH], ortho-aminobenzoic (o-ABA), (1-ethyl-3-(3-dimethylaminopropyl)carbodiimide (EDC), N-hydroxysuccinimide (NHS), ethanolamine (EtNH<sub>3</sub>), phosphate-buffered saline (PBS) pellets, anhydrous ethanol, bovine serum albumin (BSA), anti-bovine serum albumin (aBSA), streptavidin, biotin, hexaammineruthenium (III) trichloride ([Ru(NH<sub>3</sub>)<sub>6</sub>]Cl<sub>3</sub>) and sulfuric acid (H<sub>2</sub>SO<sub>4</sub>) were purchased from Sigma-Aldrich and were used without any further purification. Gold electrodes (100 nm thick) were electron beam evaporated on a substrate consisting of 280 nm of SiO<sub>2</sub> on silicon.

*SAM functionalization.*—The gold electrodes were cleaned with acetone, methanol, and isopropanol rinses and dried with  $N_2$ . The electrodes were then incubated for a range of incubation time (2–24 h) in an ethanolic thiol solution of various concentrations in piranhacleaned (3:1 96%  $H_2SO_4/H_2O_2$ ) glass Petri dishes. The SAM-functionalized gold electrodes were prepared in a  $N_2$  atmosphere provided by a Labstar Pro glovebox (MBRAUN), with  $H_2O$  and  $O_2$  both <1 ppm. After incubation, the electrodes were sonicated for 5 min in fresh ethanol, followed by drying in a stream of  $N_2$ .

o-ABA functionalization.—The gold electrodes were cleaned with acetone, methanol, and isopropanol rinses and dried with  $N_2$ . The substrates were placed in a solution containing 50 mM ortho-aminobenzoic acid in  $H_2SO_4$ . The carboxylated film was deposited via 10 cyclic voltammetry scans (0–0.8 V vs Ag/AgCl, 50 mV s<sup>-1</sup>). The substrates were rinsed with distilled water and dried with  $N_2$ .

**Receptor attachment.**—The BSA protein (1% in PBS) was immobilized onto the SAM-functionalized gold electrode through amine coupling using a 0.1 M NHS and 0.4 M EDC mixture in a 1:1 ratio by volume. Electrodes were incubated for 20 min in this NHS/EDC solution. Following incubation, electrodes were rinsed with DI water, followed by PBS. Electrodes were then incubated in 1% BSA solution for 30 min. Following BSA attachment, electrodes were rinsed with PBS, followed by DI water. Lastly, the electrodes were blocked and deactivated using 1 M ethanolamine-HCl, pH 8.5 solution for 30 min.

*EIS measurements.*—Faradaic EIS measurements were conducted in 1X PBS (pH 7.4) buffer solutions containing 1 mM [Ru(NH<sub>3</sub>)<sub>6</sub>]Cl<sub>3</sub> at room temperature. A three-electrode system was used, consisting of a dip-in Ag/AgCl reference electrode and a gold counter electrode. The area of the working electrode was  $\sim$ 0.25 cm<sup>2</sup>.

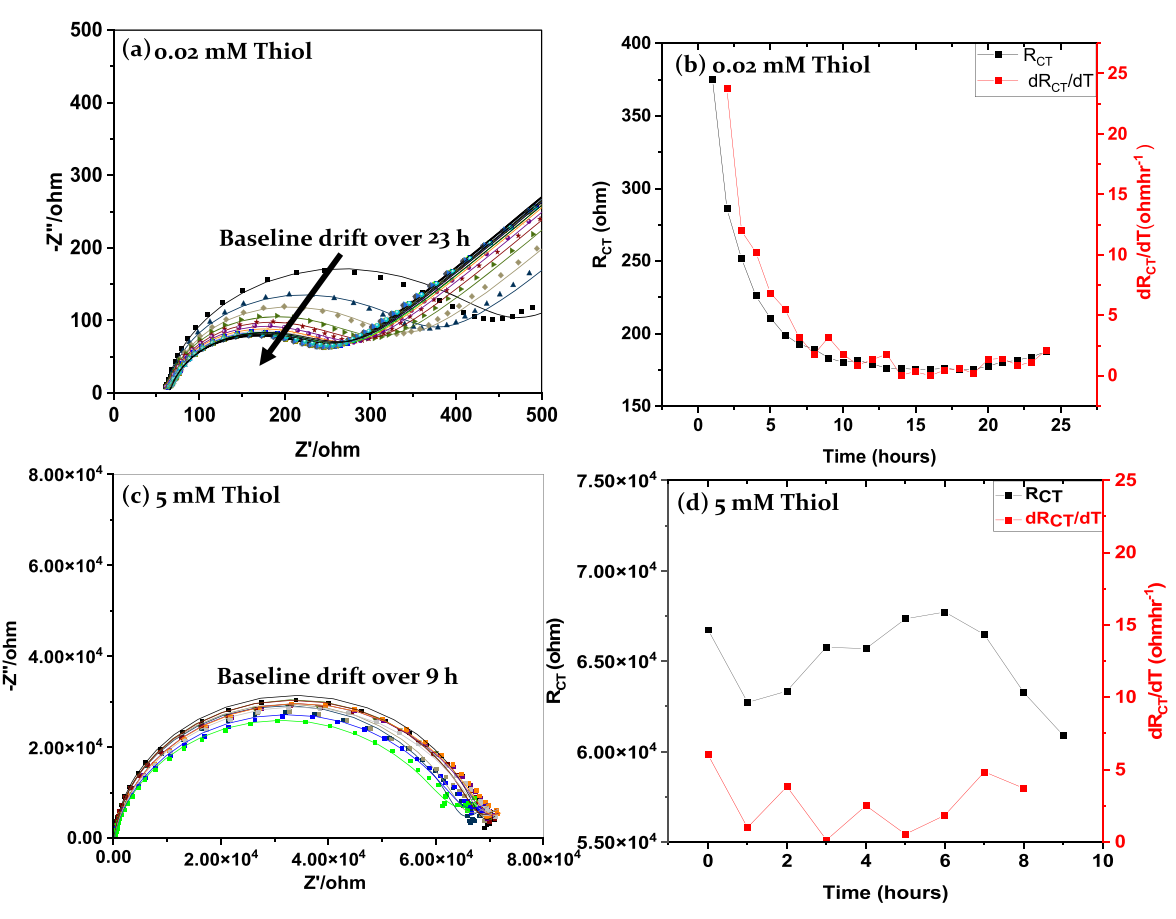


Figure 1. (a) Nyquist plots for 16-mercaptohexadecanoic acid SAM functionalized gold electrodes formed using a 0.02 mM ethanolic thiol solution. The EIS measurements were performed every hour for 23 h. (b)  $R_{CT}$  and  $dR_{CT}/dt$  as a function of measurement time extracted using an equivalent circuit model from the Nyquist plots in (a). (c) Nyquist plots for 16-mercaptohexadecanoic acid SAM functionalized gold electrodes formed using a 5 mM ethanolic thiol solution. The EIS measurements were performed every hour for 9 h. (d)  $R_{CT}$  and  $dR_{CT}/dt$  as a function of measurement time extracted using an equivalent circuit model from the Nyquist plots in (c).

The area of the working electrode that was submerged into the measurement buffer was measured and marked with a diamond scribe. The mark was made on the silicon wafer. Additionally, the volume of the measurement buffer was kept constant throughout these measurements. A frequency range from 100 kHz to 0.1 Hz at 10 points per decade was used. The AC potential amplitude was set to 5 mV vs the open circuit potential at an applied DC potential of -0.17 V for the thiol-functionalized gold electrodes, and -0.4 V for the o-ABA functionalized gold electrodes.

*XPS characterization.*—Electrode characterization was conducted using a K-Alpha X-ray photoelectron spectrometer system (Thermo Scientific, Waltham, MA) with a monochromatic Al Kα source (KE = 1486.6 eV), a 180° double focusing hemispherical analyzer, and a 128-channel detector. High resolution elemental spectra were acquired at a pass energy of 50 eV and a spot size of 400 μm. XPS spectra were fit using a previously developed protocol.  $^{33,34}$  All spectra were fit using a Shirley type background.  $^{33,34,44}$  The Au 4 f spectra were fit with 2 peaks (spin–orbit splitting of 3.7 eV, 3:4 area ratio), with the 4f7/2 peak position used as a reference at 84 eV. Two chemical states were used to fit the sulfur spectra, S–Au and S–H, which we have previously shown to signify properly and improperly bound sulfur to gold, respectively.  $^{33}$  S 2p spectra were fit with two peaks, corresponding to two binding states (spin–orbit splitting of 1.16 eV, 1:2 area ratio).  $^{33}$  The S–Au peak is found in the 161.8–162.0 eV range.  $^{33,34,43,44}$  Therefore, the corresponding  $^{20,12}$  peak was allowed to optimize within that range. The improperly bound sulfur peak is

reported over a wider range, 163–164.2 eV.<sup>33,34,43,44</sup> Therefore, the peak position was unconstrained.<sup>33</sup> The constraint for the full width half max for the improperly bound sulfur peak was set to that of the properly bound sulfur.<sup>33</sup>

## **Results and Discussion**

*Drift in R<sub>CT</sub> for SAM-functionalized gold electrodes.*—Figure 1 shows typical results of Faradaic EIS measurements performed every hour on SAM-functionalized electrodes. Figures 1a and 1c show Nyquist plots for SAM functionalized gold electrodes that were incubated for 24 h in .02 mM and 5 mM ethanolic thiol solutions, respectively. At high frequencies, a semicircle is observed where the diameter corresponds to the charge transfer resistance. At low frequencies, a 45° straight line is observed corresponding to the Warburg impedance. The Warburg impedance is associated with the diffusion of the redox species towards the working electrode. An equivalent circuit model was used to extract the R<sub>CT</sub> from the EIS data as described in the supplementary material (Fig. S1 (available online at stacks.iop.org/ECSSP/1/031605/mmedia)). The extracted charge transfer resistance and the magnitude of the change in R<sub>CT</sub> with time (dR<sub>CT</sub>/dt) is shown in Figs. 1b and 1d for the .02 mM and 5 mM ethanolic thiol solutions, respectively. For the case of the SAM formed using .02 mM ethanolic thiol solution, the EIS measurements typically show significant baseline drift for the first  $\sim$ 9 h of consecutive EIS measurements. The EIS measurements for SAM functionalized gold electrodes formed using 5 mM ethanolic thiol solutions typically showed a decrease in the magnitude of the baseline drift.

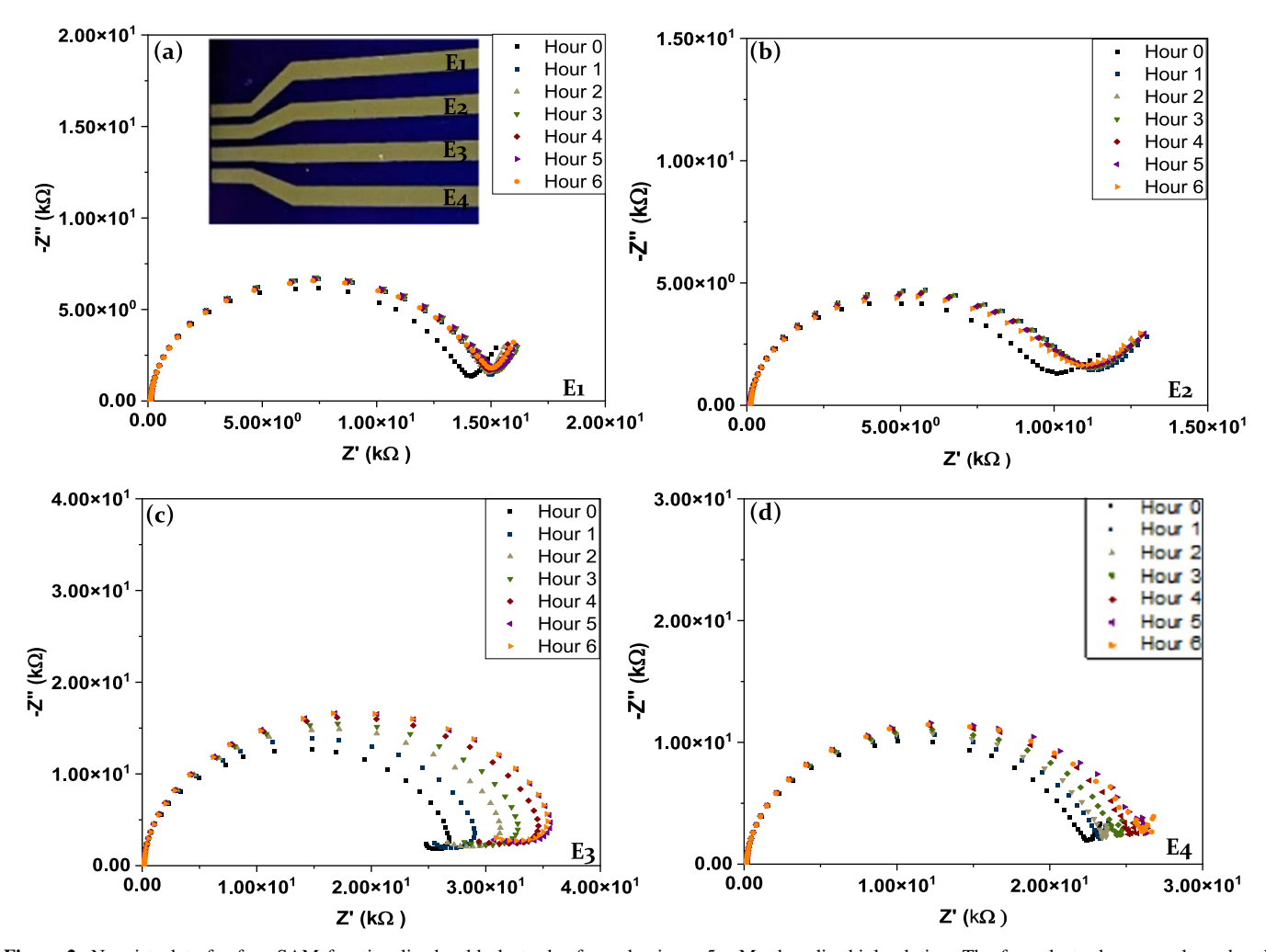


Figure 2. Nyquist plots for four SAM functionalized gold electrodes formed using a 5 mM ethanolic thiol solution. The four electrodes were cleaned and incubated in the same ethanolic thiol solution for 24 h. The magnitude of drift in  $R_{CT}$  was observed to vary significantly from one electrode to the next.

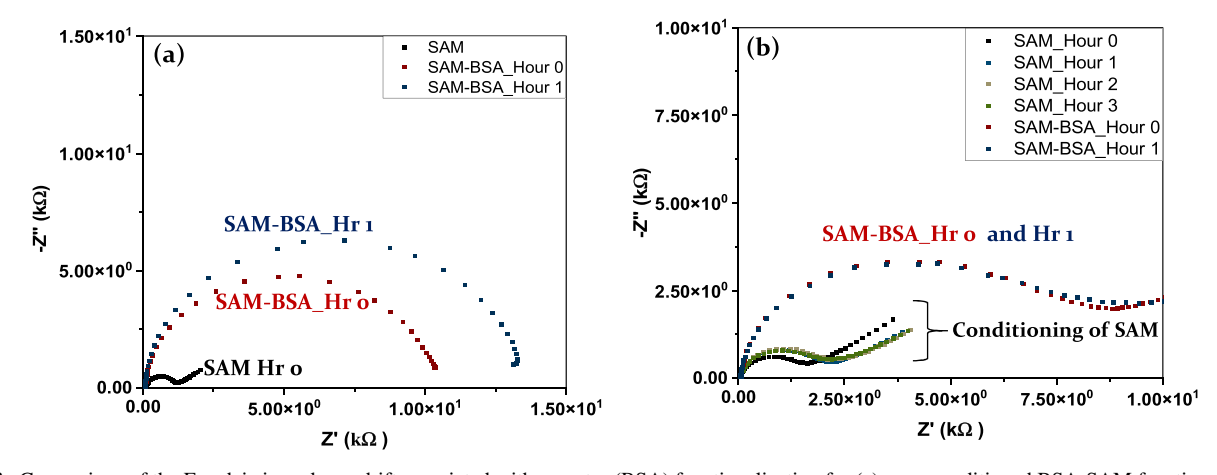


Figure 3. Comparison of the Faradaic impedance drift associated with receptor (BSA) functionalization for (a) an unconditioned BSA-SAM functionalized gold electrode vs (b) a pre-conditioned BSA-SAM functionalized gold electrode.

Although, there is an observed correlation between the concentration ethanolic thiol solution and the observed baseline drift, the magnitude of the baseline drift was found to vary from one electrode to the next. Figure 2 shows Nyquist plots for four electrodes functionalized in a 5 mM ethanolic thiol solution. These four gold electrodes were fabricated via electron beam evaporated on the same substrate consisting of 280 nm of SiO<sub>2</sub> on silicon. Following,

fabrication, the electrodes were cleaned and placed into the same ethanolic thiol solution for 24 h. Electrodes 1 and 2 reached a stable  $R_{\rm CT}$  baseline after two hours of measurements, while electrodes 3 and 4 did not reach a stable  $R_{\rm CT}$  after 6 h of consecutive measurements. Despite an identical experimental protocol being used to prepare these thiol-based SAM functionalized gold electrodes, there was considerable variability in the observed magnitude

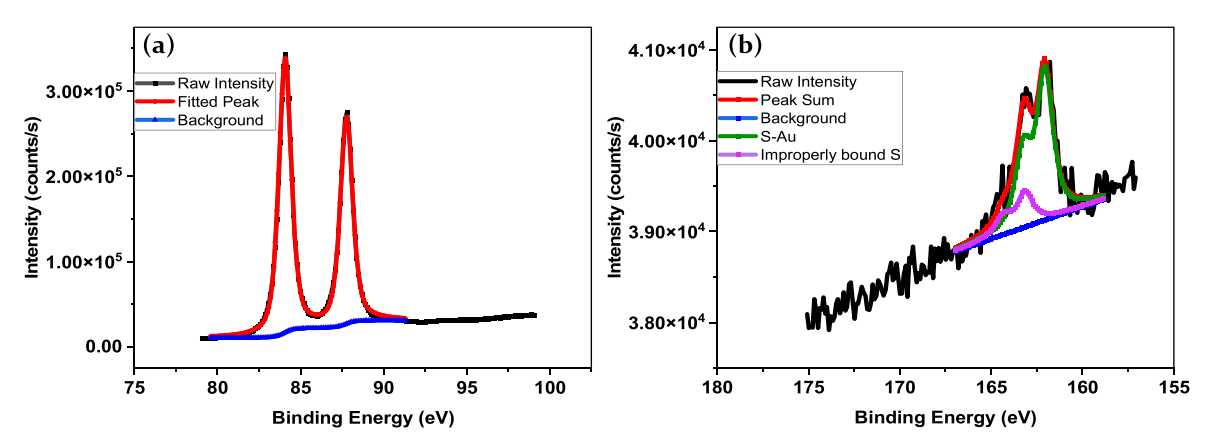
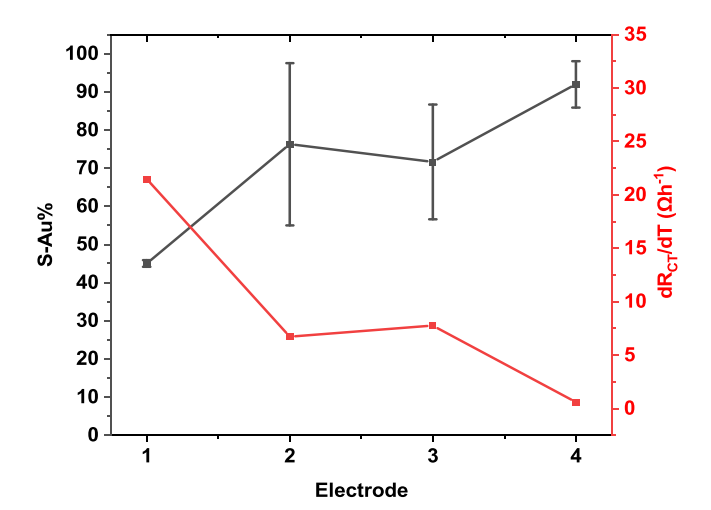


Figure 4. Example of the XPS fitting used for the SAM functionalized gold electrodes. (a) XPS fitting for the gold electrode spectra. (b) XPS fitting for the properly and improperly bound sulfur to the gold area.



**Figure 5.** The  $R_{CT}$  values were extracted from fitting the data illustrating the baseline  $R_{CT}$  drift observed for four separate electrodes to the equivalent circuit model. The rate of change in  $R_{CT}$ , and the percentage of properly bound S–Au is plotted as a function of the respective electrode.

of the baseline drift. The relationship between the magnitude of the baseline drift and the SAM incubation time (2–24 h) was also investigated as summarized in Fig. S2. The magnitude of the baseline drift varied for all the incubation times. Thus, highlighting the challenges associated with gold electrodes functionalized using thiol-based SAMs.

Importance of the Conditioning Step Prior to Receptor Attachment.—The R<sub>CT</sub> drift in the receptor functionalized SAM electrodes correlated to the baseline drift in the SAM functionalized gold electrodes. Previous publications have shown cases where the R<sub>CT</sub> baseline drift was greater in magnitude than the change in R<sub>CT</sub> associated with the attachement of the target analyte.<sup>27</sup> Thus compromising the reliability of this measurement technique. Conditioning of the SAM functionalized gold electrode prior to receptor functionalization was found to suppress the baseline drift. This allowed for stable EIS measurements associated with receptor functionalization. Figure 3a illustrates the typical biosensing experimental protocol, whereby a freshly prepared SAM functionalized gold electrode was activated and functionalized with the receptor protein. To observe the stability and reproducibility of the EIS measurements associated with the receptor functionalized SAM, EIS measurements were repeated every hour for two hours in the measurement solution.

Figure 3a illustrates the drift associated with the receptor functionalized SAM. Alternatively, Fig. 3b shows that stable R<sub>CT</sub>

measurements associated with the receptor functionalized SAM electrode is achieved after conditioning of the SAM functionalized gold electrode to reach a stable  $R_{\rm CT}$  baseline. EIS measurements were performed on a SAM functionalized gold electrode every hour until the drift in the extracted  $R_{\rm CT}$  was suppressed and stable. The subsequent EIS measurements associated with receptor attachment was observed to be stable. Although a stable baseline, achieved through conditioning of the SAM functionalized Au, results in a stable  $R_{\rm CT}$  associated with receptor functionalization, the time necessary to reach this stable baseline is unknown. Thus, this protocol is unreasonable for real sensing applications. While a conditioning step can be used to reduce the magnitude of drift in  $R_{\rm CT}$ , the conditioning time and associated drift is variable suggesting that conditioning is not a practical solution for PoCTs.

Impact of SAM composition and bonding on EIS baseline drift.—Prior results by Xu et al. had shown significant baseline drift in EIS for gold electrodes functionalized with mercaptohexanol, a short chain length alkanethiol. <sup>27</sup> It was hypothesized that the observed baseline drift was related to the non-uniformity of the SAM. The longer chain SAMs used here (16-mercaptohexadecanoic acid) should be more uniform and densely packed as compared to the shorter chain mercaptohexanol-based SAMs as these long chain alkanethiols reduce cooperative hydrogen bonding between neighboring carboxy-terminated functional groups by increasing the spatial separation between neighboring thiol molecules. <sup>26,30</sup>Additionally, the longer alkyl chains increases the chain-to-chain Van der Waals interactions, thus increasing the crystallinity and packing density of the SAM. <sup>26,30</sup>

To determine the impact of SAM composition on the EIS baseline drift, XPS was performed on the 16-mercaptohexadecanoic acid SAM functionalized gold electrodes. The obtained gold and sulfur spectra were fit using XPSpeak software<sup>33</sup> and a previously developed fitting protocol described in the methods.<sup>33</sup> Figure 4 shows a typical XPS spectra for the (a) Au  $4f_{7/2}$  and the (b) S  $2p_{3/2}$  peaks.

Figure 5 shows the relationship between the magnitude of the baseline R<sub>CT</sub> drift (dR<sub>CT</sub>/dT), and the surface composition of the gold electrodes as characterized by XPS. XPS was performed on three sample spots on each electrode to quantify the percentage of S-Au as a percentage of the total sulfur content. The magnitude of the baseline drift is observed to be inversely related to the percentage of S-Au as characterized via XPS. Additionally, the percentage of properly bound sulfur to gold is shown to vary greatly across the across the area of these electrodes, as signified by the large error bars. A high percentage of improperly bound sulfur to gold results in an increase in the electrostatic repulsions between the neighboring alkyl thiol molecules. In theory this increase in electrostatic repulsions results in a higher degree of reorganization resulting in a larger magnitude of the measured baseline drift. Therefore, it is hypothesized that the higher the percentage of properly bound sulfur to gold, the less reorganization of the thiol molecules in solution.

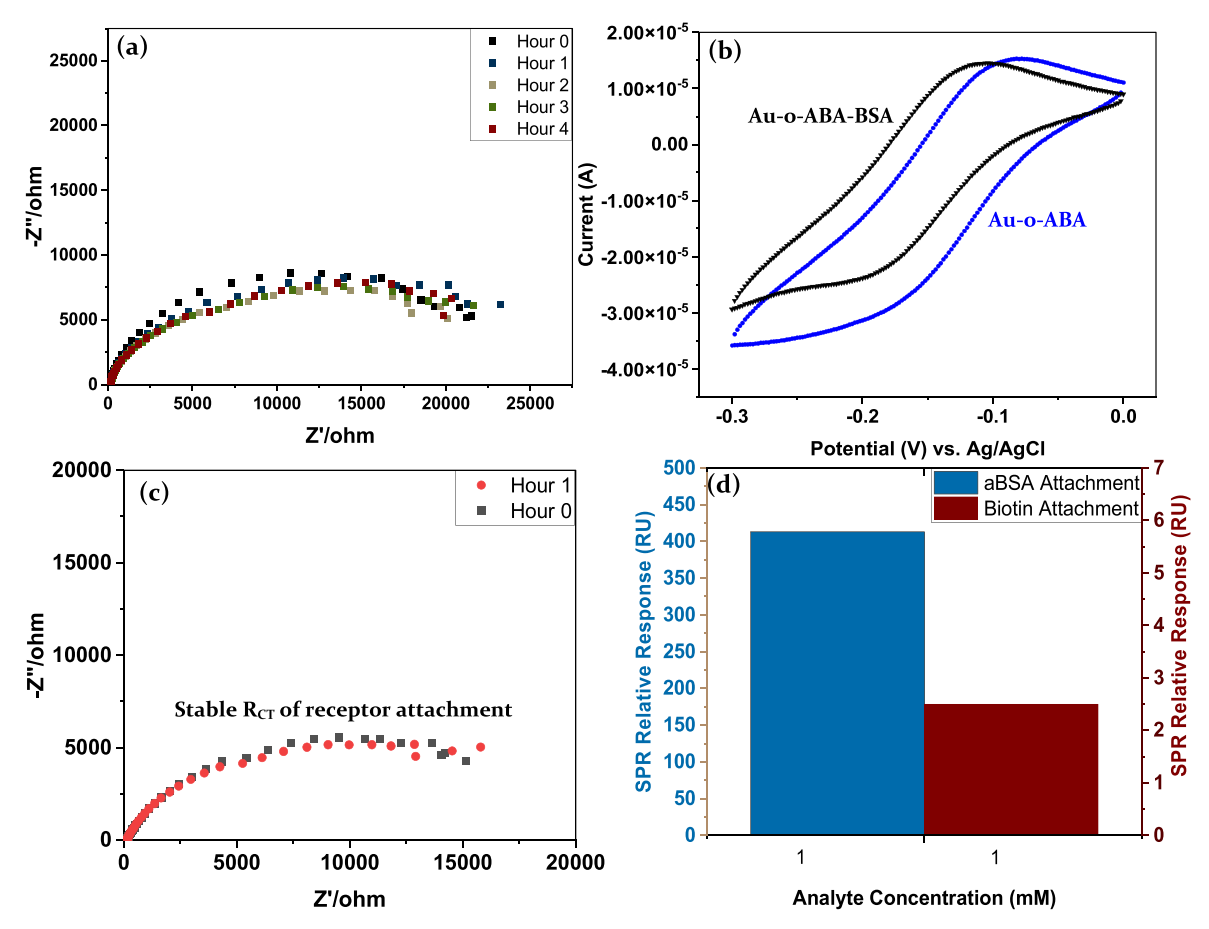


**Figure 6.** Nyquist plots for the electrode with a 1 h interval between measurements.(a) Faradaic impedance drift for the o-ABA-functionalized gold electrode in the measurement buffer solution containing 1 mM Hexaammineruthenium(III) Trichloride at room temperature. (b) Cyclic Voltammograms showing the redox peaks of the o-ABA functionalized gold electrode and the subsequent suppression of the redox peaks after receptor protein functionalization (c) Nyquist plots showing the stability of the receptor attachment to an o-ABA functionalized gold electrode over two hours without the incorporation of a conditioning step. (d) SPR Relative Response for the aBSA and Biotin attachment onto active BSA and Streptavidin receptor proteins respectively.

This ultimately results in negligible drift in the measured  $R_{\rm CT}$  as is shown in Fig. 5. Although a high percentage of properly bound S to Au, was found to correlate to negligible drift in the measured  $R_{\rm CT}$ , consistently forming a SAM that has a high percentage of properly bound S to Au was challenging. This suggests the need for a surface linker molecule where stability is not heavily dependent on electrostatic repulsions between neighboring molecules.

Suppression of EIS Baseline Drift in o-ABA-Functionalized Gold Electrode.—To address the issues associated with SAM-functionalized gold electrodes, a polymer-based surface linker (o-ABA) was investigated. This polymer has carboxyl-terminal functional groups, which allows for the functionalization of a receptor protein via amine reactive cross-linker chemistry. This polymer functionalized gold electrode was deposited via electrodeposition using 10 cycles of cyclic voltammetry. The electrodeposition of this polymer based surface linker via cyclic voltammetry is shown in the SI, Fig. S3.

Figure 6a shows a typical Nyquist plot obtained for the polymer functionalized gold electrodes. Similar stability and reproducibility was observed for three additional electrodes shown in Fig. S4, where a stable baseline is achieved between 0–1 h of stabilization measurements. Additionally, cyclic voltammograms of the o-ABA functionalized gold electrodes in the measurement buffer have been shown in Fig. S4 for each of the respective electrodes. This offers a significant improvement to the drift observed utilizing thiol based surface linkers. Cyclic Voltammetry was used to confirm the functionalization of the receptor protein to the polymer based surface linker. Figure 6b shows the redox peaks of the o-ABA functionalized

gold electrode and the subsequent suppression of these peaks after receptor functionalization. Additionally, Fig. 6c shows that stability of the polymer functionalized electrodes leads to the subsequent stability in the measured R<sub>CT</sub> associated with the receptor functionalization. In contrast to SAM functionalized gold electrodes, the polymer functionalized gold electrodes do not require the incorporation of a conditioning step prior to receptor attachment in order to achieve stable R<sub>CT</sub> measurements. It is hypothesized that the associated stability of these polymer functionalized gold electrodes is associated with the structure of this linear polymer chain, which has covalent bonds between neighboring aromatic groups. These covalent bonds, in addition to  $\pi$  to  $\pi$  stacking of the aromatic rings, do not allow for the deposited polymer to easily reorganize. Thus, by selecting a surface linker that is not dependent on the percentage of properly bound S-Au and the subsequent electrostatic repulsions between neighboring alkyl chains, the baseline drift was found to be effectively suppressed. Figure 6d shows the receptor activity of BSA and streptavidin once they were functionalized onto the o-ABA-Au electrodes via amine reactive cross-linker chemistry. This illustrates the practical application of o-ABA functionalized gold electrodes in biosensors for use in PoCT.

Although thiol based SAMs are commonly used for biosensor applications, they have been shown to have a limited shelf-life. This is due to the high propensity for the S-Au bond to oxidize under ambient conditions. 33,34,45,46 The oxidation of the S-Au bond leads to the desorption of the thiol molecules, which decreases the uniformity of the SAM. A variety of methods have been developed to mitigate the oxidation of this S-Au bond. More recently, alternative surface linkers, namely N-heterocyclic carbenes

(NHCs) have been shown to have improved stability as these surface linkers do not depend on the S-Au bond to adsorb onto the gold electrode. 47-49 Similarly, o-ABA, does not depend on the S-Au bond to adsorb onto the gold electrode. Therefore, it is hypothesized that the limited shelf-life associated with thiol functionalized gold electrodes can be improved through the use of the o-ABA functionalized gold electrodes. To test this hypothesis, future work entails elucidation of the degradation mechanism and the subsequent shelf-life of these polymer based surface linkers. The o-ABA functionalized gold electrodes have been shown to suppress the baseline drift associated with impedimetric biosensing. In addition to stability, the sensitivity of these biosensors is an important parameter to optimize. Short chain alkanethiol functionalized gold electrodes have shown improved EIS sensitivity in comparison to longer chain alkanethiols.<sup>52</sup> This is due to the lower starting R<sub>CT</sub> produced by the shorter chain alkanethiols. However, shorter chain alkanethiols form less uniform SAMs. 30,31 Thus, the increase in sensitivity observed when using shorter alkanethiols is accompanied by a decrease in the stability and reproducibility associated with the sensor response. Alternatively, the o-ABA functionalized sensor surface can be used to improve the sensitivity of the sensor, whilst maintaining the stability and subsequent reproducibility of the sensor response. To achieve this, future work involves characterization and optimization of the adsorbed polymer film thickness via ellipsometry to ensure a thin polymer layer, whilst maintaining high surface coverage.

### **Conclusions**

The stability of two classes of surface linkers were studied, where their ability to suppress faradaic EIS baseline drift was compared.

The baseline drift was found to correlate to the drift in the receptor functionalized electrode. Hence, suppression of the baseline drift is necessary for stable and reproducible electronic biosensing. The stability of SAM-functionalized gold electrodes was found to depend on the percentage of S bound to Au. To utilize these SAM functionalized gold electrodes, a conditioning step is required for stable EIS measurements. This conditioning step is dependent on the percentage of properly bound S-Au; however, the percentage of properly bound S-Au was found to vary despite identical experimental protocol being used. Thus, limiting the ability to standardize this protocol.

To address this problem, the stability of a polymer based surface linker, namely ortho-aminobenzoic acid was investigated. These polymer functionalized gold electrodes, while still allowing sensor functionalization through amine coupling, successfully suppressed the EIS baseline drift. This effective suppression of the baseline drift correlated to the stability associated with the receptor attachment without the need for the conditioning step. Thus, this class of polymer based surface linkers offers an ideal alternative to the conventionally used thiol based SAMs for stable EIS measurements.

## Acknowledgments

This work was supported in part the Agriculture & Food Research Initiative Tri-partite Competitive Grant no. 2018-67015-28307 from the USDA National Institute of Food and Agriculture; Department of Agriculture, Environment and Rural Affairs, Northern Ireland; and, Department of Agriculture, Food and the Marine, Ireland; the Marcus Center for Therapeutic Cell Characterization and Manufacturing; The Georgia Foundation; and the Georgia Research Alliance. This work was performed in part at the Georgia Tech Institute for Electronics and Nanotechnology, a member of the National Nanotechnology Coordinated Infrastructure, which is supported by the National Science Foundation (Grant ECCS-1542174). This material is based upon work supported by the National Science Foundation Graduate Research Fellowship under Grant No. DGE-1650044. The authors declare that they have no known competing financial interests or personal relationships that could have appeared to influence the work reported in this paper.

## **ORCID**

Hilena F. Gezahagne https://orcid.org/0000-0002-2344-0741

#### References

- 1. R. S. Yalow and S. A. Berson, J. Clin. Invest., 39, 1157 (1960).
- 2. C. M. Miraglia, J Chiropr Med, 15, 272 (2016).
- S. I. Stoeva, J.-S. Lee, J. E. Smith, S. T. Rosen, and C. A. Mirkin, J. Am. Chem. Soc., 128, 8378 (2006).
- M. Hu, J. Yan, Y. He, H. Lu, L. Weng, S. Song, C. Fan, and L. Wang, ACS Nano, 4, 488 (2010).
- D. A. Hall, R. S. Gaster, T. Lin, S. J. Osterfeld, S. Han, B. Murmann, and S. X. Wang, *Biosens. Bioelectron.*, 25, 2051 (2010).
- Y. Wang, Y. G. Zhou, M. Poudineh, T. S. Safaei, R. M. Mohamadi, E. H. Sargent, and S. O. Kelley, *Angew. Chem. Int. Ed. Engl.*, 53, 13145 (2014).
- 7. Z. Zhang, Y. Guan, M. Li, A. Zhao, J. Ren, and X. Qu, *Chem. Sci.*, 6, 2822 (2015).
- 8. N. Nath and A. Chilkoti, Anal. Chem., 76, 5370 (2004).
- 9. J. Homola, Anal Bioanal Chem, 377, 528 (2003).
- X. Li, S. Song, Q. Shuai, Y. Pei, T. Aastrup, Y. Pei, and Z. Pei, *Scientific Reports*, 5, 14066 (2015).
- S. Bhattacharya, J. Jang, L. Yang, D. Akin, and R. Bashir, J. Rapid Methods Autom. Microbiol., 15, 1 (2007).
- 12. R. Bogue, Sensor Rev., 27, 7 (2007).
- 13. Y. Cui, Q. Wei, H. Park, and C. M. Lieber, Science, 293, 1289 (2001).
- I. Park, Z. Li, A. P. Pisano, and R. S. Williams, *Nanotechnology*, 21, 015501 (2009).
- F. Patolsky, G. Zheng, O. Hayden, M. Lakadamyali, X. Zhuang, and C. M. Lieber, *Proc. Natl Acad. Sci.*, 101, 14017 (2004).
- T.-S. Pui, A. Agarwal, F. Ye, Z.-Q. Tou, Y. Huang, and P. Chen, *Nanoscale*, 1, 159 (2009).
- E. Stern, A. Vacic, N. K. Rajan, J. M. Criscione, J. Park, B. R. Ilic, D. J. Mooney, M. A. Reed, and T. M. Fahmy, *Nat. Nanotechnol.*, 5, 138 (2010).
- 18. B. R. Takulapalli, ACS nano, 4, 999 (2010).
- 19. S. K. Yoo, S. Yang, and J. Lee, Nanotechnology, IEEE Transactions on, 7, 745 (2008).
- E. Stern, J. F. Klemic, D. A. Routenberg, P. N. Wyrembak, D. B. Turner-Evans, A. D. Hamilton, D. A. LaVan, T. M. Fahmy, and M. A. Reed, *Nature*, 445, 519 (2007).
- 21. E. Stern, A. Vacic, and M. A. Reed, IEEE Trans. Electron Devices, 55, 3119 (2008).
- E. Stern, R. Wagner, F. J. Sigworth, R. Breaker, T. M. Fahmy, and M. A. Reed, *Nano Lett.*, 7, 3405 (2007).
- W. Hong, S. Lee, E. Jae Kim, M. Lee, and Y. Cho, *Biosens. Bioelectron.*, 78, 181 (2016).
- 24. J. S. Daniels and N. Pourmand, *Electroanalysis*, 19, 1239 (2007).
- 25. M.-Y. Tsai et al., Appl. Phys. Lett., 111, 073701 (2017).
- J. C. Love, L. A. Estroff, J. K. Kriebel, R. G. Nuzzo, and G. M. Whitesides, *Chem. Rev.*, 105, 1103 (2005).
- X. Xu, A. Makaraviciute, S. Kumar, C. Wen, M. Sjödin, E. Abdurakhmanov, U. H. Danielson, L. Nyholm, and Z. Zhang, *Anal. Chem.*, 91, 14697 (2019).
- 28. Y. Xue, X. Li, H. Li, and W. Zhang, *Nat. Commun.*, **5**, 4348 (2014)
- A. Butterworth, E. Blues, P. Williamson, M. Cardona, L. Gray, and D. K. Corrigan, Biosensors, 9, 22 (2019).
- R. R. San Juan, M. S. Miller, M.-A. Ferrato, and T. B. Carmichael, *Langmuir*, 28, 13253 (2012).
- 31. N. K. Chaki and K. Vijayamohanan, *Biosens. Bioelectron.*, **17**, 1 (2002).
- L. Jiang, C. S. S. Sangeeth, L. Yuan, D. Thompson, and C. A. Nijhuis, *Nano Lett.*, 15, 6643 (2015).
- E. L. Brightbill, B. Hitchcock, M.-Y. Tsai, A. Verga, and E. M. Vogel, *The Journal of Physical Chemistry C*, 123, 16778 (2019).
- E. L. Brightbill, H. F. Gezahagne, D. S. Jin, B. Brown, and E. M. Vogel, *Appl. Surf. Sci.*, 557, 149843 (2021).
- 35. H. Wang, S. Chen, L. Li, and S. Jiang, Langmuir, 21, 2633 (2005).
- 36. R. Arnold, W. Azzam, A. Terfort, and C. Wöll, *Langmuir*, 18, 3980 (2002).
- A. R. Cardoso, F. T. C. Moreira, R. Fernandes, and M. G. F. Sales, *Biosens. Bioelectron.*, 80, 621 (2016).
- J. A. Ribeiro, C. M. Pereira, A. F. Silva, and M. G. F. Sales, *Biosens. Bioelectron.*, 109, 246 (2018).
- S. Z. Mousavisani, J. B. Raoof, R. Ojani, and Z. Bagheryan, *Bioelectrochemistry*, 122, 142 (2018).
- 40. G. Henihan et al., Biosens. Bioelectron., 81, 487 (2016).
- 41. B. Lakard, Applied Sciences, 10, 6614 (2020).
- N. Robinson, R. Creedon, E. Sayers, Kennedy, and A. O'Riordan, *Anal. Methods*, 12, 2655 (2020).
- 43. R. Arnold, A. Terfort, and C. Wöll, *Langmuir*, 17, 4980 (2001).
- S. Frey, V. Stadler, K. Heister, W. Eck, M. Zharnikov, M. Grunze, B. Zeysing, and A. Terfort, *Langmuir*, 17, 2408 (2001).
- 45. J. B. Schlenoff, M. Li, and H. Ly, J. Am. Chem. Soc., 117, 12528 (1995).
- 46. M. H. Schoenfisch and J. E. Pemberton, J. Am. Chem. Soc., 120, 4502 (1998).
- 47. C. M. Crudden et al., Nat. Chem., 6, 409 (2014).
- 48. C. M. Crudden et al., Nat. Commun., 7, 12654 (2016).
- Z. Li, K. Munro, I. I. Ebralize, M. R. Narouz, J. D. Padmos, H. Hao, C. M. Crudden, and J. H. Horton, *Langmuir*, 33, 13936 (2017).
- 50. P. Kanyong, C. Catli, and J. J. Davis, Anal. Chem., 92, 4707 (2020).
- L. Srisombat, A. C. Jamison, and T. R. Lee, Colloids and Surfaces A: Physicochemical and Engineering Aspects, 390, 1 (2011).
- V. Anandan, R. Gangadharan, and G. Zhang, Sensors (Basel), 9, 1295 (2009).